Thesis for The Degree of Licentiate of Engineering

Characteristics of Vertical Forest Backscatter Profiles Measured using Radar Tomography

Patrik Bennet

Department of Space, Earth and Environment
Chalmers University of Technology
Gothenburg, Sweden, 2023

Characteristics of Vertical Forest Backscatter Profiles Measured using Radar Tomography

Patrik Bennet

Department of Space, Earth and Environment
Division of Geoscience and Remote Sensing
Chalmers University of Technology
SE-412 96 Göteborg,
Sweden
Phone: +46(0)31 772 1000

Cover:
Tomographic synthetic aperture radar tomogram of a temperate forest in Nationalpark Eifel, Germany. The image is showing backscatter at L-band in dB and the colour-scale ranges over 15 dB. The measurement was done as a part of the European Space Agency TomoSense campaign.

Printed by Chalmers Digitaltryck,
Gothenburg, Sweden 2023.

Characteristics of Vertical Forest Backscatter Profiles Measured using Radar Tomography

PATRIK BENNET

Department of Space, Earth and Environment
Chalmers University of Technology

Abstract

Forests are an integral part of the Earth's climate system, having shaped the conditions of life throughout millions of years, but the coverage and conditions of forests are under rapid change. To monitor this change and predict the impact on climate, yearly global mapping of forest Above-Ground Biomass (AGB) is needed. Synthetic Aperture Radar (SAR) is a well-suited technique for this purpose, able to sense through dense canopies with high spatial resolution.

Tomographic SAR (TomoSAR) resolves the vertical distribution of backscatter by constructing 3D tomograms of forested areas. Here, results obtained in the TomoSense project are presented, where sensitivity of P- and L-band TomoSAR to AGB of a temperate forest is analysed. For the first time, differences between the AGB dependence of spruce and beech vertical backscatter profiles are identified. Moreover, unique observations of ground slope influence on TomoSAR AGB retrieval are presented. The effect for P-band is significant, but not for L-band. For spruce, AGB was estimated for P-/L-band (ground slopes below 10°), with $R^2 = 0.86/0.75$ and RMSE = 15.6/12.5%. Without separating forest types, $R^2 = 0.77/0.54$ and RMSE = 11.4/12.0%.

Finally, unique L-band radar tomography observations using the BorealScat tower-based radar are presented. Time series of the vertical backscatter profile of a boreal forest during the summer of 2018 is analysed. Weekly diurnal cycles up to 1.3 dB are observed, showing clear differences depending on both canopy height layer and polarization. These differences are new results which are likely related to tree transpiration phenomena but needs further study.

Keywords

Forest remote sensing, radar tomography, P-band, L-band, above-ground biomass, temporal backscatter variations, vertical reflectivity profiles

List of Publications

Appended papers

This thesis is based on the following publications:

[**Paper I**] S. Tebaldini, M. Mariotti D'Alessandro, L. M. H. Ulander, **P. Bennet**, A. Gustavsson, A. Coccia, K. Macedo, M. Disney, P. Wilkes, H.-J. Spors, N. Schumacher, J. Hanuš, J. Novotný, B. Brede, H. Bartholomeus, A. Lau, J. van der Zee, M. Herold, D. Schuettemeyer and K. Scipal, *"TomoSense: A unique 3D dataset over temperate forest combining multi-frequency mono- and bi-static tomographic SAR with terrestrial, UAV and airborne lidar, and in-situ forest census".*
Remote Sensing of Environment, vol. 290, p. 113532, 5 2023.

[**Paper II**] **P. J. Bennet**, L. M. H. Ulander, M. Mariotti D'Alessandro and S. Tebaldini, *"Sensitivity of P- and L-band SAR tomography to above-ground biomass in a hilly temperate forest".*
IEEE Transactions on Geoscience and Remote Sensing. Submitted.

[**Paper III**] **P. J. Bennet**, A. R. Monteith and L. M. H. Ulander, *"Diurnal cycles of L-band tomographic SAR backscatter in a boreal forest during summer: Observations by the BorealScat tower radar".*
2023 IEEE International Geoscience and Remote Sensing Symposium (IGARSS), Pasadena, CA, USA, 7 2023. Accepted for publication.

Acknowledgment

First and foremost, I want to thank my supervisor Lars Ulander for his wise guidance and always constructive feedback. Through your strategic decisions, you ensure that the research progresses, with a clear sense of both risk-taking and restraint. I feel great appreciation for my assistant supervisor Albert Monteith, for your incessant passion for research, pedagogical explanations, practical experience and humour. Thanks to your hard and skilled work, I've had the tomographic radar time series data from the BorealScat tower radar to delve into. I also want to thank my assistant supervisor Johan Fransson, for your great interest in the research and unceasing energy to push forward.

Many people were involved in the European Space Agency (ESA) TomoSense campaign, where I worked the closest with Stefano Tebaldini and Mauro Mariotti d'Alessandro at Politecnico di Milano. Thanks to their good work processing the TomoSAR data, I could do the analysis in Paper II. And thanks to the airborne lidar scanning done by CzechGlobe, I had an AGB reference for the TomoSAR data. Also, the field inventory data collected by Landesbetrieb Wald und Holz proved important both for generating the AGB reference map and for separating forest types in the analysis. I am grateful for having had the opportunity to be part of such a unique project together with all of you.

Thank you to my colleagues at the Division of Geoscience and Remote Sensing, and especially to you fellow PhD students. Together we can brighten up and ease this intense and challenging time in our lives.

Finally, a big thank you to my dear family, my mother, father and sisters, for constantly supporting me to pursue my own path and showing me love.

My work has been funded by the European Space Agency (ESA, contract no. 4000127285/19/NL/FF/gp), Vetenskapsrådet (VR, dnr 2019-05289) and the Swedish Research Council (FORMAS, dnr 2020-01961).

Contents

Part I

Summary

Chapter 1

Introduction

1.1 The Role of Forests in the Global Climate

Forests play a central role in shaping the Earth's climate. At the time when our Homo Sapiens species evolved and started burning them to create open lands or viewing them as a material resource, forests had through millions of years set up and stabilized the conditions for life on our planet [1], [2]. Trees are among the longest living organisms known to us, with several existing specimen being several thousand years old [3]. The fact that they can accomplish this while standing stationary, trapped in a pile of soil, suggests that we have a lot to learn from trees when it comes to sustainable resource management.

Before the industrial revolution, about one twelfth of atmospheric carbon was exchanged by forests each year, in a cycle of carbon uptake and release, accounting for 50% of terrestrial photosynthesis [4]. Subsequent changes in anthropogenic emissions, tropical deforestation and forest fertilization (due to a higher atmospheric concentration of CO_2) have disrupted this balance of atmospheric carbon exchange. Between year 1700 and today, the total coverage of forest has reduced from about 37% to 31% of the land area [5]. The rate of loss has reduced since the 1990s, largely due to an increased area of plantation forest [6], but future widespread loss is anticipated due to current changes in global climate [7].

The World Meteorological Organization (WMO), in cooperation with other organizations, have identified a set of Essential Climate Variables (ECVs) needed to model and predict the trajectory of climate [8]. Forests have an integral role for the ECVs summarized in Table 1.1. Their importance for the biosphere is apparent, e.g. by being host to among the most bio-diverse ecosystems, being vital for oxygen production and enriching soils with nutrients. They act as a global carbon sink and account for a large part of the carbon flux, but our knowledge of the distribution and amount of forest biomass is far from comprehensive [9]. To reach acceptable uncertainties, global Above-Ground dry Biomass (AGB) mapping with annual repetitions is necessary. To achieve this, satellite missions are deemed necessary. An example is the European Space Agency (ESA) BIOMASS mission, which will bring the very first P-band

Observing system	**ECVs**
Carbon cycle	Carbon dioxide
...	Above-ground dry biomass
...	Soil carbon
Biosphere	Oxygen
...	Nutrients
...	Leaf area index
...	Land cover
...	Fraction of absorbed photosynthetically active radiation
Hydrological cycle	Evaporation from land
...	Surface water vapour
...	Soil moisture
...	Groundwater
...	Precipitation
Energy balance	Land surface temperature
...	Surface air temperature
...	Albedo
Composition and transport	Surface wind speed & direction
...	Aerosols

Table 1.1: Forest-related ECVs and the part of the climate system they observe.

(432-438 MHz) Synthetic Aperture Radar (SAR) instrument into orbit [10].

Perhaps not as often appreciated, forests interact strongly with the hydrological cycle involving ECVs such as evaporation from land, soil moisture and precipitation. Through photosynthesis, vegetation binds carbon from the atmosphere and releases oxygen, but this process requires significant amounts of water vapour. The daily water use of tropical tree species with tree diameters of 34 to 98 cm was estimated to about 40 to 800 liters per tree [11]. Furthermore, the presence of natural tropical forest slows groundwater flows, thereby balancing its level during dry periods, and increases its rate of recharge compared to a tree savanna [12]. Water also evaporates from the ground surface and upon the interception of rain. The total water vapour release is a function of both evaporation from the ground, canopy intercepted precipitation and transpiration, collectively referred to as Evapo-Transpiration (ET). The water transferred to the atmosphere via ET, in combination with released aerosols from the trees, enhance cloud formation and precipitation directly over the forest itself and in surrounding regions [13].

The energy balance of the Earth is modulated by the low albedo of forests and the cooling effect of ET [14]. Forests are carbon neutral or carbon sinks, which also contributes to a global net cooling effect. Tropical forests are estimated to have a net cooling effect, due to their high ET, while the global influence of temperate and boreal forests remain uncertain. The relatively low ET and low albedo (compared to snow cover) of boreal forests even suggests that their presence contribute to net global warming, but at the same time are

Technique	**Observables**
Optical	Surface reflectance and spectrum:
...	*VIs, FAPAR, LAI, SOC, SIF, albedo, biomass*
Lidar	Height and density of returns:
...	*Vertical structure, LAI, biomass*
SAR	Backscatter, coherence, polarization and VOD:
...	*Vertical structure, biomass*

Table 1.2: Important techniques for global forest remote sensing, with respective observables and related biophysiological variables. Included abbreviations: Synthetic Aperture Radar (SAR), Vegetation Index (VI), Fraction of Absorbed Photosynthetically Active Radiation (FAPAR), Leaf-Area Index (LAI), Soil Organic Carbon (SOC), Sun Induced Fluorescence (SIF) and Vegetation Optical Depth (VOD).

a large part of the terrestrial carbon sink [14].

Many feedbacks between forests and the global climate system are still unexplored and the reliability of climate models are limited by the uncertainties or lack of coverage of current forest-related ECV measurements. When it comes to monitoring and modelling the global carbon budget, the amount of carbon storage and disturbance in tropical forests is believed to have the largest uncertainty [15].

1.2 Forest Monitoring

Many different techniques are used to monitor the Earth's forests. They estimate a number of biophysiological parameters assessing the health, composition and dynamics of forest ecosystems, each with respective limitations. Three main cathegories of techniques can be identified: remote sensing, field surveys and inventories, and in-situ sensor systems. Only satellite remote sensing techniques are feasible for global forest monitoring, since the pure scale of the problem and its corresponding resource requirements rules out all other options. Reviews of terrestrial carbon cycle monitoring using remote sensing and flux towers are covered in [16] and also for the hydrological cycle in [15]. Aerial and terrestrial techniques are reviewed in [17]. Remote sensing applications to forest biodiversity are covered in [18].

Important techniques for global remote sensing, with respective observables and related estimated biophysiological variables, are summarized in Table 1.2. Remote sensing methods include passive techniques, such as photography/spectral imaging and microwave radiometry, and active techniques, such as lidar and radar. The fundamental difference between passive and active techniques is that active techniques provide their own illumination and thereby rely on utilizing their control of the transmitted signal properties. As a consequence, spaceborne SAR sensors are able to acquire far superior resolution (meters) compared to passive radiometric sensors (kilometers). Additionally, cloud cover is a limitation of optical sensors, while clouds are transparent for microwave sensors. There still remains potential to further improve and extend the measurement capabilities of forest monitoring techniques. For example, P-band radar has shown sensitivity to forest transpiration processes [19], which may enable new forest vitality and hydrological observations.

Usually, local observations from field surveys or inventories and in-situ sensors are used to develop models which relate the remote sensing observations to the biophysical parameters of interest. Among ground-based systems, the global networks of eddy-covariance flux towers are especially important for monitoring forest ecosystem carbon, water and energy exchange [16]. In-situ forest water dynamics is usually monitored using semi-invasive sensors such as dendrometers, sap-flow sensors, soil-moisture sensors and flow sensors in water sheds. Forest species and biomass inventories typically includes traditional diameter-at-breast-height (DBH) measurements, tree height and tree count within randomized plot areas [20]. Furthermore, sophisticated Terrestrial Laser Scanning (TLS) techniques are evolving, including mobile and UAV platforms [16]. TLS is able to provide very detailed information of the forest structure by constructing proper 3D images of the forest where species, stems, branches and leaves are segmented.

1.3 Objectives

The work presented herein aims to improve the understanding of how tomographic radar techniques can be used to estimate forest biophysiological properties and processes. More specifically, prospects of relating the observations to forest biomass and water dynamics is assessed. This is of importance for evaluating Tomographic SAR (TomoSAR) as a technique for future global forest carbon stock and flux monitoring as well as for investigating its sensitivity to ET processes by connecting observations to microwave scattering and forest hydrology models. The goals of this work were to

- Evaluate the sensitivity of P- and L-band TomoSAR observations to temperate forest above-ground dry biomass and assess related nuisance factors, as a part of the TomoSense ESA campaign (Papers I and II).
- Investigate the BorealScat tower radar L-band tomographic radar time series observations and how they relate to the temporal water dynamics of the forest (Paper III).

The next chapter will provide a brief introduction to the theory and practice of tomographic radar forest remote sensing. First, radar tomography basics are covered, followed by theory and examples of how the radar signal interacts with the forest environment. This includes the effects of dielectric properties and scattering mechanisms on radar backscatter. Thereafter, experimental observations of the influence of forest biophysiological properties and processes on temporal and spatial variations of tomographic radar backscatter is summarized.

Chapter 2

Remote Sensing of Forests using Radar Tomography

2.1 Radar Tomography

A radar system can measure the ratio of power returning to the radar from a resolution cell relative to the power transmitted to the cell, i.e. the backscatter of a surface or volumetric resolution cell in the scene [21]. Tomographic synthetic aperture radar (TomoSAR) techniques provides vertical resolution and thus enables more precise observations of the vertical distribution of backscatter [22]. In research on radar tomography of forests, dependencies of the temporal and spatial characteristics of the vertical distribution of backscatter are analysed. The goal is to identify and properly understand the connection between the radar measurements and forest biophysiological properties.

2.1.1 Radar Principles

The most basic principle of a radar is to transmit a radio pulse and record the arrival time of echoes from the environment. A measured time delay t is converted to a range measure ρ by relating to the speed of light c as

$$\rho = \frac{ct}{2}. \tag{2.1}$$

The attainable resolution in distance is the range resolution and is given by [23]

$$\delta_\rho = \frac{c}{2B}, \tag{2.2}$$

where B is the pulse (or system) bandwidth around the carrier frequency. The operating frequency band of a radar system is referred to according to a system of intentionally unrelated letters. Table 2.1 summarizes a few of these, including name, frequency range and wavelength.

Band	**Frequency**	**Wavelength**
VHF	3 - 300 MHz	10 - 1 m
P	216 - 450 MHz	139 - 67 cm
UHF	0.3 - 1 GHz	100 - 30 cm
L	1 - 2 GHz	30 - 15 cm
S	2 - 4 GHz	15 - 7.5 cm
C	4 - 8 GHz	7.5 - 3.75 cm
X	8 - 12 GHz	3.75 - 2.5 cm
Ku	12 - 18 GHz	2.5 - 1.7 cm
K	18 - 27 GHz	1.7 - 1.1 cm
Ka	27 - 40 GHz	1.1 - 0.75 cm
V	40 - 75 GHz	7.5 - 4 mm
W	75 - 110 GHz	4 - 2.7 mm
mm	110 - 300 GHz	2.7 - 1 mm
THz	0.3 - 1 THz	1 - 0.3 mm

Table 2.1: Radar frequency bands and corresponding wavelengths according to IEEE standard 521-2019.

A radar signal incident over an area or object can be expressed as a Fourier series expansion with time-harmonic electromagnetic (EM) plane wave components, each with a phasor (i.e. a complex number representation) form

$$\vec{E} = (\hat{v}E_v + \hat{h}E_h)e^{-jk\hat{k}\cdot\vec{R}}, \tag{2.3}$$

where $\hat{v}$ and $\hat{h}$ are unit vectors such that $\hat{h}$ lies in a plane parallel to ground, with both vectors orthogonal to each other and the wave propagation direction $\hat{k}$ [21]. That is, $\vec{E}$ consists of a vertical polarization component $\hat{v}E_v$ and a horizontal polarization component $\hat{h}E_h$, where the amplitudes are complex valued (j is the imaginary unit). k is the wave number and $\vec{R}$ describes the radial distance and direction from the EM wave source. If the radar transmits a pulse that is vertically polarized and also measures the received vertically polarized power, it is said to measure the VV (vertical-vertical) power. Similarly, a horizontally polarized transmit and receive measurement is abbreviated as HH. The leftmost and the rightmost letter denotes the receive and transmit polarization respectively. The two possible cross-polarized measurements are thus HV and VH.

The Radar Cross Section (RCS) σ_{pq} at a polarization pq, where p and q are V or H, of an object is the ratio of the power of the backscattered EM wave $\vec{E}_s^p$ relative to the power of that incident $\vec{E}_i^q$ [24]. It is defined as

$$\sigma_{pq} = \lim_{\rho\to\infty} 4\pi\rho^2 \frac{|\vec{E}_s^p|^2}{|\vec{E}_i^q|^2}. \tag{2.4}$$

$\rho \to \infty$ implies that the antenna is located in the far-field of the scatterer and that the scattered EM wave can be approximated as spherical. The ratio of backscatter from a surface σ_{pq}^0 or volume σ_{pq}^v within a resolution cell, such as from soil or a vegetation cover, to the respective surface area or volume is commonly referred to as the backscattering coefficient or the radar reflectivity [21]. It is defined similarly to Equation (2.4) and expressed normalized by the area A or volume V of coverage as

$$\sigma^0_{pq} = \frac{< \sigma_{pq} >}{A}, \tag{2.5}$$

or

$$\sigma^v_{pq} = \frac{< \sigma_{pq} >}{V}, \tag{2.6}$$

where $< \cdot >$ denotes the statistical average.

Any radar system observing scenes where several objects or rough surfaces are present in a resolution cell, such as usually in natural environments, is affected by speckle noise. This type of noise is caused by the (from an observation point of view) random constructive and destructive superposition of reflections from multiple scatterers within a resolution cell. The power of such noise is exponentially distributed and thereby its standard deviation proportional to the average observed intensity (i.e. to the backscatter coefficient) [21], [25]. It is often the dominant disturbance in radar observations of natural environments. The residual standard deviation of the backscatter coefficient due to speckle noise, $s_{speckle}$, is inversely proportional to the square root of the number of independent samples N_s used in the averaging procedure as [21]

$$s_{speckle} = \frac{< I >}{\sqrt{N_s}}, \tag{2.7}$$

where I is the observed intensity. Moving of the antenna such that the radar return of the forest volume decorrelates can also be used to acquire more independent samples to further suppress the speckle noise.

2.1.2 Tomographic Synthetic Aperture Radar

Radar range measurements taken from different positions, such as along a line when an airplane, drone or satellite carrying the radar instrument is moving along its trajectory, can be combined to construct a synthetic aperture larger than the physical antenna [22]. The positions of measurements can be arbitrary, but linear apertures are often practical and straightforward to apply theory to. In general, several trajectories of radar measurements, such as from consecutive flights along closely-spaced parallel tracks as is shown in Figure 2.1, builds up a sparse 3D synthetic aperture antenna. The 2D projection of this antenna aperture as seen from a position on the ground will determine the resolution in azimuth and elevation, as is illustrated in Figure 2.1. Resolution in range is already provided by the pulse bandwidth, resulting in a 3D imaging capability.

Assuming parallell line trajectories with equispaced sample points and baselines (distance between trajectories), the following results of resolution can be derived. The resolution in the azimuth dimension, as given in [23], corresponds to

$$\delta_{az} = \frac{\lambda}{2\theta_{int,az}} \tag{2.8}$$

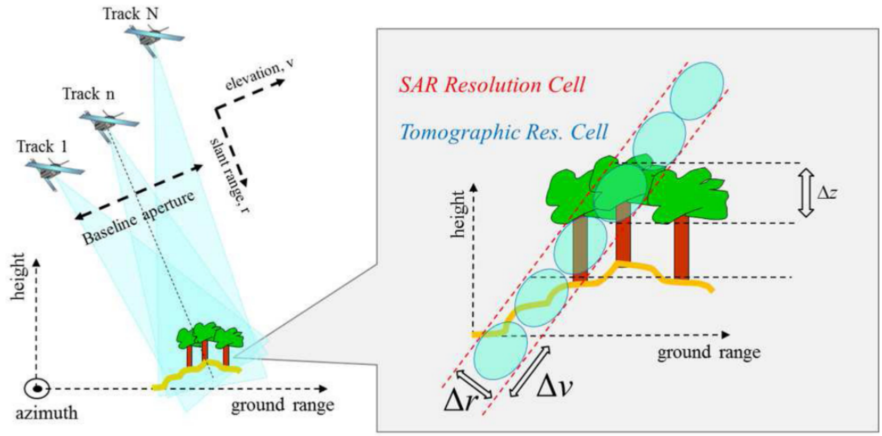

Figure 2.1: Illustration of a TomoSAR acquisition geometry and the resulting resolution cells compared to that of SAR (a single flight track). Δr is the range resolution, Δv the elevation resolution and Δz the corresponding vertical resolution. ©2011 IEEE. Reprinted, with permission, from [26].

and the resolution in the vertical dimension is given by [22], [27] as

$$\delta_z = \frac{\lambda\rho}{2L_B}\sin\theta. \tag{2.9}$$

where λ is the wavelength, $\theta_{int,az}$ the synthetic aperture integration angle in the azimuth dimension, ρ the slant range, θ the look angle (the angle from zenith in the resolution cell to the antenna aperture) and L_B the baseline of the aperture in the elevation dimension.

Common techniques to compute a TomoSAR tomogram from the radar range profiles at each sample point are backprojection, Fourier beamforming, Capon beamforming and compressive sensing [27]–[29]. Backprojection and Fourier beamforming conserve the radiometric accuracy of the image, while Capon beamforming and compressive sensing are methods that can acquire vertical super-resolution (i.e. better than that of Equation (2.9)) but at the cost of decreasing radiometric stability.

2.2 Dielectric Properties

An EM wave propagating in a medium or incident on an object is attenuated and scattered due to induced electric currents. The mechanism of these currents is a combination of ohmic conduction and charge displacement currents. The alignment of polar molecules to the electric field of the EM wave causes displacement currents. Since the field is oscillating, charges are in motion, i.e. in current. In natural environments such as the troposphere, ocean, grassland, bare soil or forests, the main conducting substance for radio- and microwaves is water. Its presence dominates the value of the complex dielectric constant, which controls the attenuation in a media and reflection at (or transmission through) a surface. Observing these environments, the radar instrument is sensitive to water. In a forest, water is present everywhere - in the stems, branches and leaves of trees and other vegetation as well as in the ground soil. All these are components that build up a complex three-dimensional structure which the radar signal is sensitive to.

The dielectric properties of a material describes how an incident EM wave induces movement of charge and heat dissipation in the material. This is encapsuled in the complex dielectric constant ϵ, defined (for isotropic materials) as

$$\epsilon = \epsilon_0 \epsilon_r = \epsilon_0(\epsilon' - j\epsilon''), \tag{2.10}$$

where ϵ_r is the relative dielectric constant, which consists of ϵ', the relative permittivity, describing the displacement of charge causing an induced electric field, and the dielectric loss factor ϵ'', which accounts for the energy transfer from the EM wave to the material [30].

The dielectric properties of soil are highly dependent on the soil moisture content. At a frequency of 1.4 GHz and a variation of volumetric soil moisture content of 0 to 50 %, ϵ_r varies from about $2.5 - j0$ to $35 - j8$ [32], with ϵ' eventually approaching that of water at about 77 [33]. The level of salinity in water mostly affects the dielectric loss factor at frequencies below 10 GHz [30]. The dielectric loss factor ϵ'' varies as much as from 4 to 90 between pure and sea water at 1 GHz. As temperatures dive below zero, water forms into ice and ϵ_r changes drastically. Pure ice has a loss factor ϵ'' below about 10^{-3} in the 1 to 10 GHz range [30]. ϵ' is almost independent of temperature and frequency in this region, with a value of about 3.2. So, ice is virtually transparent and close to lossless in the P- to X-band frequency range usually considered for radar remote sensing of forests.

Vegetation dielectric properties are dependent on the volumetric water content. E.g. for corn leaves with a volumetric water content varying from 0 to 60 %, ϵ_r changed from 0 to about $40 - j15$ [34]. The dielectric constant of tree trunks is known to vary on a diurnal scale. A time series measurement from [31] of P-band ϵ_r change at four heights in a Norway spruce (*Picea abies* [L.] Karst) tree is shown in Figure 2.2. The ϵ_r of tree trunks is dependent on depth from its surface, polarisation (hence it is not isotropic) and tree species. These diurnal variations of tree trunks are supposedly related to tree water content and its change due to transpiration activity.

2.3 Scattering Mechanisms

Not only is the EM wave interaction with the forest environment dependent on the dielectric properties of materials, it also depends on their geometry. Even if the dielectric properties of the material would be constant with frequency, the geometry strongly determines the scattering properties. The backscatter dependency on object size d is often divided into three scattering zones: Rayleigh scattering ($d << \lambda$), Mie scattering ($d \approx \lambda$) and geometrical optics scattering

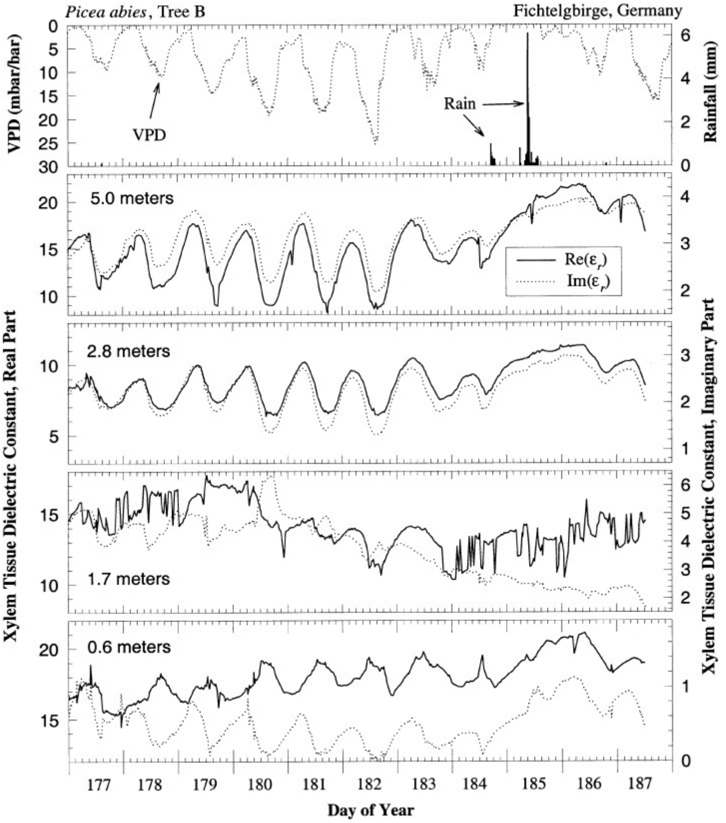

Figure 2.2: Plots of Vapour-Pressure Deficit (VPD) (an indicator of favourable transpiration conditions), rainfall, relative dielectric constant real part ϵ' and imaginary part ϵ'' at P-band and at four heights in the stem of a Norway spruce (*Picea abies* [L.] Karst) tree. The VPD reference is set to the top of the graph, normalized to the standard atmospheric conditions at sea level (1013 mbar). ©2002 IEEE. Reprinted, with permission, from [31].

($d >> \lambda$) [35]. For objects smaller than the wavelength, i.e. for Rayleigh scattering, the backscatter is proportional to λ^{-4} and is thus weak. Therefore, radars operating at different frequencies are sensitive to structures of different size in the forest. E.g. leaves and smaller branches in the forest canopy strongly reflects an X-band signal with 3 cm wavelength, while they are transparent for a P-band signal with 70 cm wavelength [36]. Although, attenuation is proportional to λ^{-1} and can still be significant for a layer of distributed particles [35]. Moreover, objects with large and smooth surfaces (compared to the wavelength) cause coherent scattering (the wave is reflected with a uniform wavefront) that is strong in the specular direction (i.e. it acts like a mirror). Conversely, rough and randomly structured objects cause incoherent scattering that add up constructively or destructively randomly in any direction (causing the speckle effect). In terms of sensor parameters, the reflection on

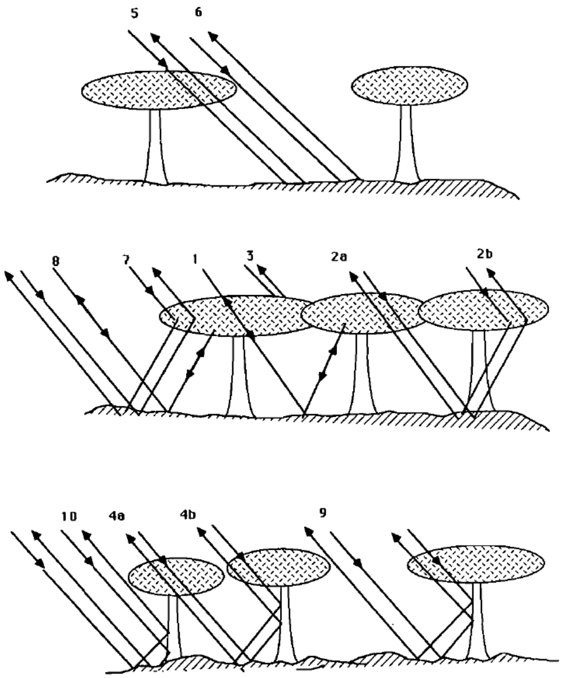

Figure 2.3: Illustration from [37] of backscatter components in a forest, subject to different combinations of scattering mechanisms.

and transmission through surfaces and structures depends on the polarization, wavelength and incidence angle of the EM wave.

As the microwave radar signal propagates through the complex forest canopy structure, it is subject to a vast number of single- and multiple-scattering events. This dilutes its power density, which also reduces due to heat losses [35]. The power of the forest backscatter observed by the radar is dominated by the lower order scattering terms. EM scattering models of forest consider a number of components contributing to the total backscatter, as is illustrated in Figure 2.3. An example of a forest scattering model is MIMICS [37], [38], which has been applied in e.g. [39]–[46]. A computation of L-band backscatter using this model is shown in Figure 2.4. A polarisation dependence is seen, where the largest difference is due to the ground-trunk double-bounce contribution.

Three key mechanisms involved in the forest backscatter, in addition to absorption, can be mentioned: Fresnel reflection, Bragg scattering and dihedral scattering. First, forward scattering from a plane wave incident on a dielectric surface is described by the Fresnel reflection scattering mechanism [35]. The strength and polarisation of the reflected wave is dependent on the dielectric properties of the material and the incidence angle, but the HH reflection is in general stronger than the VV reflection for a horizontal surface. The Fresnel reflection assumes a specular reflection, i.e. for a smooth surface. Slight surface roughness, with small height variations relative to the wavelength,

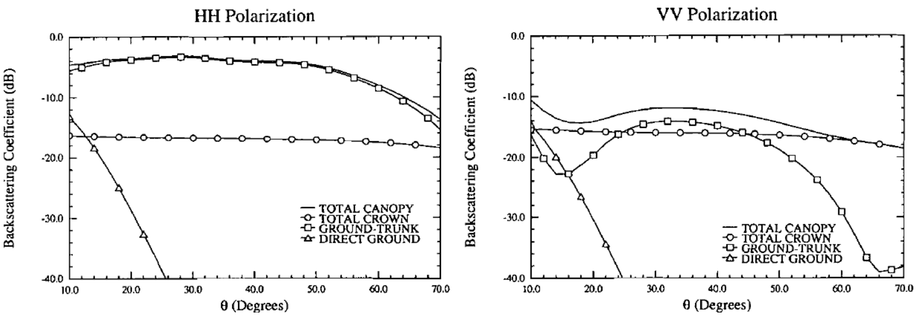

Figure 2.4: Example of simulated L-band backscatter components of a forest using the MIMICS model in [37].

can be accounted for by assuming a quasi-specular surface, which reduces the magnitude of the Fresnel reflection [35], [47]. This mechanism is involved in the ground and stem reflections of component 1, 2, 4, 7, 8, 9 and 10 in Figure 2.3.

A second important mechanism is that causing the backscattered wave from a rough dielectric surface, such as direct ground backscatter, as is involved in component 5 and 6 in Figure 2.3. Slightly electromagnetically rough surfaces (for about $2\pi\Delta s/\lambda < 0.3$, where Δs is the rms surface height) exhibit Bragg scattering, a result of approximate Fraunhofer diffraction over the random surface, while rougher surfaces approach Lambertian scattering that is isotropic in all directions [35]. Conversely to Fresnel reflection, Bragg backscatter is in general up to a few dB stronger for VV than for HH. This phenomena was observed for bare soil in e.g. [48], [49].

A third mechanism is dihedral scattering, which is the combination of two Fresnel reflections in a corner [50], possibly between two materials with different dielectric properties such as a ground layer and a tree stem. This corresponds to components 4, 9 and 10 of Figure 2.3. Just as for a single Fresnel reflection, the dihedral backscatter return is stronger for HH than for VV. Thereby, direct backscatter from the ground can be expected similar or stronger for VV than for HH, while dihedral-like structures such as the ground-trunk double-bounce implies a stronger HH backscatter. This agrees well with the simulation results of L-band backscatter contributions due to different scattering mechanisms in a forest shown in Figure 2.4.

2.4 Backscatter Variations

As has been established in the previous sections, the amount of backscatter measured by the radar from a forest under observation is caused by the biophysiological properties of that forest environment. In the case of radar tomography, the vertical distribution of backscatter is commonly referred to as the vertical reflectivity profile (VRP). In general, if excluding radar sensor parameters, spatial and temporal changes of the radar backscatter are caused by structural or dielectric variations. Over an area, the structure of the forest canopy, such as tree height, tree species, tree age and sub-canopy vegetation, or that due to forest management, contribute to forest texture variations. Moreover, topography has a significant influence on the ground backscatter and double-bounce components, and so does spatial soil moisture variations. If observing a forest area from a fixed position over time, the temporal backscatter variations are caused by changes of the value of the dielectric constant or its distribution as well as by movement of leaves, branches and stems e.g. due to wind. This includes seasonal changes, e.g. deciduous trees losing their leaves in fall or soil moisture variations and ground cover changes (caused by e.g. inundation, runoff, drought, rain or snow), and movements of stems, branches and leaves. Anthropogenic activity can of course also cause backscatter variations, deforestation being an obvious example.

2.4.1 Studies of Spatial Characteristics

TomoSAR observations of the spatial variations of the VRP in forests have mainly been done by means of airborne campaigns. The TropiSAR campaign, carried out in 2009, resulted in studies connecting the P-band VRP to tropical forest tree height, sub-canopy ground topography and the sensitivity of its variation to AGB [51]–[58]. AfriSAR was another tropical forest TomoSAR experiment, carried out in 2015-2016, with acquisitions at both P- and L-band [54], [59]–[63]. These studies have treated e.g. estimation of forest height, ground topography, 3D structure, disturbance (forest clearing) and forest AGB. The BioSAR-1 and -2 campaigns, in 2007 and 2008 respectively, provided P- and L-band results from boreal forest sites [26], [64]–[68]. The studies have covered the VRP variations relationship to boreal forest height, AGB and the influence of sloping terrain. An experiment done in Switzerland in 2006 provided a P- and L-band TomoSAR dataset over a partially forested area, where the VRP relationship to forest height, ground topography and polarimetric information was studied [69]. In 2008-2016, DLR carried out P-band and L-band TomoSAR acquisitons over a temperate forest site, providing results focused on the estimation of forest 3D structure parameters (also after the event of rain) and their use for AGB estimation [70]–[75]. In 2020, the TomoSense campaign acquired P- and L-band TomoSAR observations of a temperate forest site [76].

In general, these studies have found that the spatial variations of TomoSAR VRPs provide information well suited for estimation of forest height, ground topography, 3D structure and AGB. P-band backscatter is observed to be more sensitive to AGB than L-band, while L-band is more sensitive to forest height. Also, due to the canopy being more transparent for lower frequencies, ground topography is better observed at P-band. In addition to covering locations with different forest types and topography, differences between studies lie in implementation and system parameters such as resolution, acquisition modes, estimation methods and (radiometric and polarimetric) calibration quality. A better resolution is often possible for L-band acquisitions due to restrictions of bandwidth allocation for P-band. However, questions remain to be answered regarding the influence of e.g. soil moisture, ground slope and the mix of tree species in the forest composition.

2.4.2 Studies of Temporal Characteristics

Radar tower experiments are currently the only platforms enabling analyses of the temporal characteristics of forest backscatter on time-scales of seconds to years. Tropical forests have been observed at P-, L- and C-band by the TropiScat, TropiScat-2 and AfriScat tower radars [77]–[84]. Temporal coherence was studied on the time-scale of hours to months, where daily cycles were seen during dry days (as they were otherwise perturbed by rain) [79]–[81], [83]. Differences in the polarization dependence of the time series was also observed. Coherence dropped during mid-day, the cause being wind. The forest phase center (i.e. height of "center of mass" of the VRP) was seen to exhibit a diurnal motion vertically, with a hypothesized connection to forest ET phenomena [77]. P-band temporal decorrelation was concluded to be at a minimum at night or early morning, due to less wind and temperature changes [78]. P-band temporal coherence was also observed to vary vertically, decorrelating quicker in the forest canopy than at ground level. A significant drop of coherence was linked to the onset of transpiration activity in the morning, established by flux tower measurements [80], [81].

The BorealScat tower radar acquired multi-polarimetric P-, L- and C-band data of a boreal forest site [19], [85]–[88]. Changes of radar backscatter and temporal coherence were studied, in relation to environmental parameters. As temperatures dropped below zero, backscatter was observed to decrease 4-10 dB [85], [86]. Variations of the backscatter was also seen at times of high wind speed. P-band backscatter was observed to be more stable in the canopy than at the ground level (during non-frozen conditions) and diurnal backscatter variations were observed during hot periods, hypothesized to originate from ET phenomena [19]. Diurnal variations of P- and L-band coherence was seen, supposedly due to convective winds and ET phenomena, with minimum decorrelation at night or early morning [86].

The SodSAR experiment, a fully polarimetric SAR operating in the L- to X-band range, has provided boreal forest backscatter time series mainly in or near subzero conditions [89]–[91]. The attenuation of the forest canopy was studied, where temperature subzero-drops was observed to cause a 4 dB decrease [90]. From L-band to X-band, there was an increase of up to 18 dB in apparent two-way attenuation, with another 1-4 dB increase in attenuation with a snow covered canopy. The frequency dependence of temporal coherence in a lightly forested area was also analyzed [91].

These studies have shown that temporal variations of the VRP in a forest occur due to e.g. changing temperature, precipitation, wind and ET conditions. The influence of temperature is apparent as the backscatter and canopy attenuation reduces drastically as it drops below zero. Lower frequency bands exhibit a longer decorrelation time, i.e. stays coherent for longer times. The presence of wind causes the backscatter to decorrelate. A link between backscatter variations to transpiration activity and forest water dynamics is hypothesized, for observations of both tropical forest in dry season and boreal forest during hot summer periods.

Chapter 3

Summary of Appended Papers

3.1 Paper I: TomoSense: A unique 3D dataset over temperate forest combining multifrequency mono- and bi-static tomographic SAR with terrestrial, UAV and airborne lidar, and in-situ forest census

S. Tebaldini, M. Mariotti D'Alessandro, L. M.H. Ulander, **P. Bennet**, A. Gustavsson, A. Coccia, K. Macedo, M. Disney, P. Wilkes, H.-J. Spors, N. Schumacher, J. Hanuš, J. Novotný, B. Brede, H. Bartholomeus, A. Lau, J. van der Zee, M. Herold, D. Schuettemeyer and K. Scipal. *Remote Sensing of Environment,* Vol. 290, 15 May 2023, 113532.

This paper describes the data collected in the ESA-funded TomoSense experiment. The campaign was carried out to support research on forest remote sensing using SAR and TomoSAR at P-, L- and C-band. The data was collected over the temperate forest of the Eifel National Park in north-western Germany. The dominant species of the area were beech and spruce, with forest heights ranging from around 10 to 30 m and peaks up to 40 m. The Above-Ground dry Biomass (AGB) of the area ranges from 20 to 300 tonnes per hectare (t/ha), with peaks over 400 t/ha. A monostatic acquisition was done by a single flight for the P-band data, while both monostatic and bistatic acquisitons were done for L-band using two parallel flight tracks. Acquisitions were done in two headings, with up to 30 trajectories flown in each heading, to provide tomographic imaging capabilities. Complimentary 3D structural measurements were done via terrestrial laser scanning (TLS), unmanned aerial vehicle lidar (UAV-L) and airborne laser scanning (ALS) and in-situ forest sensus.

Contribution by P. Bennet: Results and discussion of the TomoSAR vertical reflectivity profile's AGB dependence, for spruce and beech forests separately, and AGB retrieval performance for P- and L-band. This encompasses Figures 13 and 14 and related paragraphs.

3.2 Paper II: Sensitivity of P- and L-band SAR Tomography to Above-Ground Biomass in a Hilly Temperate Forest

P. Bennet, L. M.H. Ulander, M. Mariotti D'Alessandro and S. Tebaldini. Submitted to *IEEE Transactions on Geoscience and Remote Sensing (2023).*

This paper assesses the above-ground biomass (AGB) sensitivity of the P- and L-band TomoSAR dataset acquired in the TomoSense ESA campaign. Details on the TomoSense campaign can be found in [76]. There is a knowledge gap regarding the influence of forest type (i.e. mix of tree species) and the nuisance effect of ground slopes on TomoSAR AGB retrieval capability. The TomoSAR data cover a highly topographic area, with many ground slopes above 20° and even up to 40°. It is thus well suited for ground slope nuisance analysis. The two dominant forest types of the area were beech forest and spruce forest. For the analysis, data points were divided into three forest type categories: beech, spruce and temperate (a mix of all forest types). An Airborne Lidar Scanning (ALS) estimated AGB map was used as a reference. Data points were extracted by means of a uniform grid, with each data point covering an area of 0.5 ha. The average Vertical Reflectivity Profile (VRP) of each data point was used for the sensitivity assessment.

The results show the VRP to exhibit a general dependence (in all observations) for increasing AGB, with the height of the canopy backscatter peak increasing and the intensity of the ground backscatter decreasing. Importantly, different dependencies on AGB are seen for spruce and beech forest. Spruce forest VRPs exhibit a growth in total intensity with increasing AGB, while beech forest does not. Instead, the beech forest AGB information in the VRPs is exclusively contained in the height of the upper canopy response. Another result is the evaluation of AGB retrieval performance for three different intensity retrieval methods: the total intensity I_{tot}, the 20 to 30 m canopy layer intensity I_c and the canopy-to-total ratio $I_{cr} = I_c/I_{tot}$. Note that I_{cr} is a normalized metric, i.e. the absolute intensity information is removed. The total intensity of the beech forest shows no sensitivity to AGB, while spruce forest HV is seen slightly sensitive. The retrieval based on I_c makes the benefits of TomoSAR vertical resolution evident, as all bands show sensitivity to AGB for all forest types. AGB retrieval performance for temperate forest HV at P/L-band is 38/36 t/ha RMSE (or 15/14 % relative RMSE). The normalized I_{cr} metric show a corresponding performance of 40/35 t/ha RMSE (16/13 %).

The influence of ground slope on the AGB retrieval performance is found to be significant for L-band and even more pronounced for P-band. When limiting the ground slope to below 10°, the R^2 correlation coefficient of the temperate forest P-band I_c AGB retrieval increases from 0.53 to 0.77. For this ground slope limitation the P-band R^2 increases similarly for all methods and forest types, with the most significant R^2 of 0.86 being observed for spruce forest.

3.3 Paper III: Diurnal cycles of L-band tomographic SAR backscatter in a boreal forest during summer: Observations by the BorealScat tower radar

P. Bennet, A. Monteith and L. Ulander. Accepted for publication in *2023 IEEE International Geoscience and Remote Sensing Symposium (IGARSS).* Pasadena, CA, USA, 16-21 July 2023.

Diurnal cycles in L-band tomographic radar backscatter times series acquired by the BorealScat tower radar are identified over summer 2018. This summer was a dry period in Sweden, with widespread drought leading to tree water stress and consequently bark beetle infestations. In this paper, the Vertical Reflectivity Profile (VRP) times series are shown, where the diurnal variations are present for HH and VV polarizations. The average diurnal variation per height layer is analyzed over four 7-day time intervals of interest, in May, June, April and August, representing the progression of summer. Characteristics of the vertical extent of diurnal cycles are identified, with average magnitudes up to 1.3 dB at both polarizations. They are seen to vary throughout summer and exhibit a very different behaviour for HH and VV.

The VV diurnal cycle is seen to be occurring mainly in the upper and lower forest canopy, with its maximum at night or early morning and minimum at noon. These are regions where the branch density is lower than in the middle canopy, exposing the stem more. The VV diurnal cycle is also the strongest in June and July, a period when transpiration activity is expected to be the most intense as well as a period of supposedly increasing water stress. The diurnal cycle seen at HH is, conversely, the strongest in the middle canopy, a region of high branch density. Its phase is the opposite of that seen for VV, with the HH diurnal cycle having its minimum at night and maximum at noon or early afternoon. It is also the strongest in the beginning of summer, before drought hits and the VV cycle intensifies.

These diurnal cycles are compared with Vapour-Pressure Deficit (VPD) time series, computed from in-situ measurements of air humidity and temperature. VPD is an indicator of favourable transpiration conditions. The VPD and the HH and VV diurnal variations are seen to co-vary closely, strengthening the hypothesis that tree water dynamics have an influence on L-band backscatter. The differences between the VV and HH observations are a surprising result that is yet to be properly understood.

Chapter 4

Discussion and Future Work

This thesis revolves around research done within the TomoSense and the BorealScat projects. The common denominator is the use of radar tomography to identify variations of the vertical distribution of backscatter and relate those to forest biophysiological parameters. Regarding Papers I and II, TomoSAR is reinforced as a well suited technique for forest AGB mapping. The results regarding reflectivity profile-AGB dependence, tree species dependence and ground slope nuisance indicate there to be more work to do when it comes to understanding and applying TomoSAR to forest AGB retrieval. Future work with the TomoSense dataset may focus on estimation of forest structure parameters, improving AGB estimation methods and to develop a proper understanding (including possible mitigation) of the ground slope nuisance.

Currently, the most obvious way forward is to continue the work started in Paper III. In that study, BorealScat L-band vertical reflectivity profiles exhibited diurnal cycles with clear polarization and forest layer dependence. The diurnal cycles were shown to co-vary closely with vapour-pressure deficit, likely indicating transpiration activity. The next step would be to model the vertical distribution of forest backscatter in terms of scattering mechanism components and see how well this can describe the observations (for both P- and L-band). Different models can be evaluated in terms of how well they fit the measurement data and the physical relevance of their descriptors.

The connection between components of such models to forest biophysiological processes would then be evaluated. Such components could be e.g. canopy attenuation and backscatter from branches, stems and the ground, then in combinations for different scattering mechanisms. The canopy attenuation can be measured separately, by extracting the response from a trihedral reflector located under the forest canopy, possibly providing valuable inputs to the scattering models. Furthermore, a good starting point to analyze forest scattering models in this context is to describe the significant backscatter variations seen as temperature drops below zero.

A link between radar backscatter, scattering mechanisms and forest water dynamics such as transpiration, tree water content, soil moisture and dew, will be possible to investigate more thoroughly with the new BorealScat-2 tower radar [92]. In addition to improved backscatter measurement capabilities, the incorporation of environmental data from the flux-tower in combination with extensive in-situ sensor tree physiological measurements of the observed forest will prove important for this task.

Bibliography

[1] D. K. Jha, R. Samrat and P. Sanyal, "The first evidence of controlled use of fire by prehistoric humans during the middle paleolithic phase from the indian subcontinent," *Palaeogeography, Palaeoclimatology, Palaeoecology*, vol. 562, p. 110 151, Jan. 2021. DOI: 10.1016/j.palaeo.2020.110151 (cit. on p. 3).

[2] L. Pawlik, B. Buma, P. Šamonil *et al.*, "Impact of trees and forests on the devonian landscape and weathering processes with implications to the global earth's system properties - a critical review," *Earth-Science Reviews*, vol. 205, p. 103 200, Jun. 2020. DOI: 10.1016/j.earscirev.2020.103200 (cit. on p. 3).

[3] J. Liu, S. Xia, D. Zeng *et al.*, "Age and spatial distribution of the world's oldest trees," *Conservation Biology*, vol. 36, Aug. 2022. DOI: 10.1111/cobi.13907 (cit. on p. 3).

[4] Y. Malhi, P. Meir and S. Brown, "Forests, carbon and global climate," *Philosophical Transactions of the Royal Society A: Mathematical, Physical and Engineering Sciences*, vol. 360, pp. 1567–1591, Aug. 2002. DOI: 10.1098/rsta.2002.1020 (cit. on p. 3).

[5] N. Ramankutty and J. A. Foley, "Estimating historical changes in global land cover: Croplands from 1700 to 1992," *Global Biogeochemical Cycles*, vol. 13, pp. 997–1027, Dec. 1999. DOI: 10.1029/1999GB900046 (cit. on p. 3).

[6] R. J. Keenan, G. A. Reams, F. Achard, J. V. de Freitas, A. Grainger and E. Lindquist, "Dynamics of global forest area: Results from the FAO global forest resources assessment 2015," *Forest Ecology and Management*, vol. 352, pp. 9–20, Sep. 2015. DOI: 10.1016/j.foreco.2015.06.014 (cit. on p. 3).

[7] D. M. Gates, "Climate change and forests," *Tree Physiology*, vol. 7, pp. 1–5, Dec. 1990. DOI: 10.1093/treephys/7.1-2-3-4.1 (cit. on p. 3).

[8] World Meteorological Organization (WMO), *State of the Global Climate 2022*, WMO-No. 1316. 2023. [Online]. Available: https://library.wmo.int/idurl/4/66214 (cit. on p. 3).

[9] R. A. Houghton, F. Hall and S. J. Goetz, "Importance of biomass in the global carbon cycle," *Journal of Geophysical Research: Biogeosciences*, vol. 114, Jun. 2009. DOI: 10.1029/2009JG000935 (cit. on p. 3).

[10] T. Le Toan, S. Quegan, M. W. J. Davidson *et al.*, "The BIOMASS mission: Mapping global forest biomass to better understand the terrestrial carbon cycle," *Remote Sensing of Environment*, vol. 115, pp. 2850–2860, Nov. 2011. DOI: `10.1016/j.rse.2011.03.020` (cit. on p. 4).

[11] F. C. Meinzer, S. A. James and G. Goldstein, "Dynamics of transpiration, sap flow and use of stored water in tropical forest canopy trees," *Tree Physiology*, vol. 24, pp. 901–909, Aug. 2004. DOI: `10.1093/treephys/24.8.901` (cit. on p. 4).

[12] J. Krishnaswamy, M. Bonell, B. Venkatesh *et al.*, "The groundwater recharge response and hydrologic services of tropical humid forest ecosystems to use and reforestation: Support for the "infiltration-evapotranspiration trade-off hypothesis"," *Journal of Hydrology*, vol. 498, pp. 191–209, Aug. 2013. DOI: `10.1016/j.jhydrol.2013.06.034` (cit. on p. 4).

[13] I. G. Kavouras, N. Mihalopoulos and E. G. Stephanou, "Formation of atmospheric particles from organic acids produced by forests," *Nature*, vol. 395, pp. 683–686, Oct. 1998. DOI: `10.1038/27179` (cit. on p. 4).

[14] G. B. Bonan, "Forests and climate change: Forcings, feedbacks, and the climate benefits of forests," *Science*, vol. 320, pp. 1444–1449, Jun. 2008. DOI: `10.1126/science.1155121` (cit. on pp. 4, 5).

[15] J. Worden, S. Saatchi, M. Keller *et al.*, "Satellite observations of the tropical terrestrial carbon balance and interactions with the water cycle during the 21st century," *Reviews of Geophysics*, vol. 59, Mar. 2021. DOI: `10.1029/2020RG000711` (cit. on p. 5).

[16] J. Xiao, F. Chevallier, C. Gomez *et al.*, "Remote sensing of the terrestrial carbon cycle: A review of advances over 50 years," *Remote Sensing of Environment*, vol. 233, Nov. 2019. DOI: `10.1016/j.rse.2019.111383` (cit. on pp. 5, 6).

[17] X. Liang, A. Kukko, I. Balenovic *et al.*, "Close-range remote sensing of forests: The state of the art, challenges, and opportunities for systems and data acquisitions," *IEEE Geoscience and Remote Sensing Magazine*, vol. 10, pp. 32–71, Sep. 2022. DOI: `10.1109/MGRS.2022.3168135` (cit. on p. 5).

[18] J. L. Innes and B. Koch, "Forest biodiversity and its assessment by remote sensing," *Global Ecology and Biogeography*, vol. 7, pp. 397–419, 1998. DOI: `10.1046/j.1466-822X.1998.00314.x` (cit. on p. 5).

[19] A. R. Monteith and L. M. H. Ulander, "Temporal characteristics of P-band tomographic radar backscatter of a boreal forest," *IEEE Journal of Selected Topics in Applied Earth Observations and Remote Sensing*, vol. 14, pp. 1967–1984, 2021. DOI: `10.1109/JSTARS.2021.3050611` (cit. on pp. 6, 16).

[20] B. Jonsson, J. Jacobsson and H. Kallur, "The forest management planning package. Theory and application," *Studia Forestalia Suecica*, no. 189, 1993 (cit. on p. 6).

[21] F. Ulaby, D. Long, W. Blackwell *et al.*, *Microwave Radar and Radiometric Remote Sensing*. Jan. 2014, pp. 162–225 (cit. on pp. 7–9).

[22] A. Reigber and A. Moreira, "First demonstration of airborne SAR tomography using multibaseline L-band data," *IEEE Transactions on Geoscience and Remote Sensing*, vol. 38, pp. 2142–2152, 2000. DOI: 10.1109/36.868873 (cit. on pp. 7, 9, 10).

[23] R. J. Sullivan, *Radar foundations for imaging and advanced concepts*. SciTech Publishing Inc., 2004 (cit. on pp. 7, 9).

[24] E. Knott, J. Schaeffer and M. Tulley, *Radar Cross Section* (Radar, Sonar and Navigation). Institution of Engineering and Technology, 2004, pp. 63–114 (cit. on p. 8).

[25] W. G. Rees, *Physical Principles of Remote Sensing*, 3rd ed. Cambridge University Press, 2012, pp. 281–317. DOI: 10.1017/CBO9781139017411 (cit. on p. 9).

[26] E. Blomberg, L. Ferro-Famil, M. J. Soja, L. M. H. Ulander and S. Tebaldini, "Forest biomass retrieval from L-band SAR using tomographic ground backscatter removal," *IEEE Geoscience and Remote Sensing Letters*, vol. 15, pp. 1030–1034, Jul. 2018. DOI: 10.1109/LGRS.2018.2819884 (cit. on pp. 10, 15).

[27] A. Moreira, O. Ponce, M. Nannini, M. Pardini and P. Prats, "Multibaseline imaging: A vision for spaceborne SAR," *2015 16th International Radar Symposium (IRS)*, pp. 20–29, Jun. 2015. DOI: 10.1109/IRS.2015.7226407 (cit. on p. 10).

[28] V. Cazcarra-Bes, M. Pardini, M. Tello and K. P. Papathanassiou, "Comparison of tomographic SAR reflectivity reconstruction algorithms for forest applications at L-band," *IEEE Transactions on Geoscience and Remote Sensing*, vol. 58, pp. 147–164, Jan. 2020. DOI: 10.1109/TGRS.2019.2934347 (cit. on p. 10).

[29] H. Aghababaei, G. Ferraioli, L. Ferro-Famil *et al.*, "Forest SAR tomography: Principles and applications," *IEEE Geoscience and Remote Sensing Magazine*, vol. 8, pp. 30–45, Jun. 2020. DOI: 10.1109/MGRS.2019.2963093 (cit. on p. 10).

[30] F. Ulaby, D. Long, W. Blackwell *et al.*, *Microwave Radar and Radiometric Remote Sensing*. Jan. 2014, pp. 123–161 (cit. on p. 11).

[31] K. C. McDonald, R. Zimmermann and J. S. Kimball, "Diurnal and spatial variation of xylem dielectric constant in norway spruce (Picea abies [L.] Karst.) as related to microclimate, xylem sap flow, and xylem chemistry," *IEEE Transactions on Geoscience and Remote Sensing*, vol. 40, pp. 2063–2082, Sep. 2002. DOI: 10.1109/TGRS.2002.803737 (cit. on pp. 11, 12).

[32] M. Hallikainen, F. Ulaby, M. Dobson, M. El-rayes and L. kun Wu, "Microwave dielectric behavior of wet soil-part 1: Empirical models and experimental observations," *IEEE Transactions on Geoscience and Remote Sensing*, vol. GE-23, pp. 25–34, Jan. 1985. DOI: 10.1109/TGRS.1985.289497 (cit. on p. 11).

[33] T. Meissner and F. J. Wentz, “The complex dielectric constant of pure and sea water from microwave satellite observations,” *IEEE Transactions on Geoscience and Remote Sensing*, vol. 42, pp. 1836–1849, Sep. 2004. DOI: 10.1109/TGRS.2004.831888 (cit. on p. 11).

[34] F. T. Ulaby and R. P. Jedlicka, “Microwave dielectric properties of plant materials,” *IEEE Transactions on Geoscience and Remote Sensing*, vol. GE-22, pp. 406–415, Jul. 1984. DOI: 10.1109/TGRS.1984.350644 (cit. on p. 11).

[35] W. G. Rees, *Physical Principles of Remote Sensing*, 3rd ed. Cambridge University Press, 2012, pp. 42–109. DOI: 10.1017/CBO9781139017411 (cit. on pp. 12–14).

[36] T. Le Toan, A. Beaudoin, J. Riom and D. Guyon, “Relating forest biomass to SAR data,” *IEEE Transactions on Geoscience and Remote Sensing*, vol. 30, pp. 403–411, Mar. 1992. DOI: 10.1109/36.134089 (cit. on p. 12).

[37] F. T. Ulaby, K. Sarabandi, K. McDonald, M. Whitt and M. C. Dobson, “Michigan microwave canopy scattering model,” *International Journal of Remote Sensing*, vol. 11, pp. 1223–1253, Jul. 1990. DOI: 10.1080/01431169008955090 (cit. on pp. 13, 14).

[38] K. C. McDonald and F. T. Ulaby, “Radiative transfer modelling of discontinuous tree canopies at microwave frequencies,” *International Journal of Remote Sensing*, vol. 14, pp. 2097–2128, Jul. 1993. DOI: 10.1080/01431169308954024 (cit. on p. 13).

[39] K. C. McDonald, M. C. Dobson and F. T. Ulaby, “Modeling multifrequency diurnal backscatter from a walnut orchard,” *IEEE Transactions on Geoscience and Remote Sensing*, vol. 29, p. 852, Nov. 1991. DOI: 10.1109/TGRS.1991.1019469 (cit. on p. 13).

[40] P. Liang and L. Pierce, “Application of bistatic MIMICS to forest canopies,” *2004 IEEE International Geoscience and Remote Sensing Symposium (IGARSS), Anchorage, Alaska, USA*, pp. 4328–4331, Sep. 2004. DOI: 10.1109/IGARSS.2004.1370095 (cit. on p. 13).

[41] R. Ningthoujam, H. Balzter, K. Tansey *et al.*, “Relationships of S-band radar backscatter and forest aboveground biomass in different forest types,” *Remote Sensing*, vol. 9, p. 1116, Nov. 2017. DOI: 10.3390/rs9111116 (cit. on p. 13).

[42] K. C. Mcdonald, M. C. Dobson and F. T. Ulaby, “Using mimics to model L-band multiangle and multitemporal backscatter from a walnut orchard,” *IEEE Transactions on Geoscience and Remote Sensing*, vol. 28, pp. 477–491, Jul. 1990. DOI: 10.1109/TGRS.1990.572925 (cit. on p. 13).

[43] P. Liang, M. Moghaddam, L. E. Pierce and R. M. Lucas, “Radar backscattering model for multilayer mixed-species forests,” *IEEE Transactions on Geoscience and Remote Sensing*, vol. 43, pp. 2612–2626, Nov. 2005. DOI: 10.1109/TGRS.2005.847909 (cit. on p. 13).

[44] S. S. Saatchi and K. C. McDonald, "Coherent effects in microwave backscattering models for forest canopies," *IEEE Transactions on Geoscience and Remote Sensing*, vol. 35, pp. 1032–1044, Jul. 1997. DOI: 10.1109/36.602545 (cit. on p. 13).

[45] H. Israelsson, L. M. H. Ulander, T. Martin and J. I. H. Askne, "A coherent scattering model to determine forest backscattering in the VHF-band," *IEEE Transactions on Geoscience and Remote Sensing*, vol. 38, pp. 238–248, 2000. DOI: 10.1109/36.823916 (cit. on p. 13).

[46] M. L. Imhoff, "A theoretical analysis of the effect of forest structure on synthetic aperture radar backscatter and the remote sensing of biomass," *IEEE Transactions on Geoscience and Remote Sensing*, vol. 33, pp. 341–351, Mar. 1995. DOI: 10.1109/TGRS.1995.8746015 (cit. on p. 13).

[47] F. Ulaby, D. Long, W. Blackwell *et al.*, *Microwave Radar and Radiometric Remote Sensing*. Jan. 2014 (cit. on p. 14).

[48] Y. Oh, K. Sarabandi and F. T. Ulaby, "An empirical model and an inversion technique for radar scattering from bare soil surfaces," *IEEE Transactions on Geoscience and Remote Sensing*, vol. 30, pp. 370–381, Mar. 1992. DOI: 10.1109/36.134086 (cit. on p. 14).

[49] A. Freeman and S. L. Durden, "A three-component scattering model for polarimetric SAR data," *IEEE Transactions on Geoscience and Remote Sensing*, vol. 36, pp. 963–973, May 1998. DOI: 10.1109/36.673687 (cit. on p. 14).

[50] Y. Yamaguchi, Y. Yajima and H. Yamada, "A four-component decomposition of POLSAR images based on the coherency matrix," *IEEE Geoscience and Remote Sensing Letters*, vol. 3, pp. 292–296, Jul. 2006. DOI: 10.1109/LGRS.2006.869986 (cit. on p. 14).

[51] P. C. Dubois-Fernandez, T. Le Toan, S. Daniel *et al.*, "The TropiSAR airborne campaign in French Guiana: Objectives, description, and observed temporal behavior of the backscatter signal," *IEEE Transactions on Geoscience and Remote Sensing*, vol. 50, pp. 3228–3241, Aug. 2012. DOI: 10.1109/TGRS.2011.2180728 (cit. on p. 15).

[52] D. H. T. Minh, T. Le Toan, F. Rocca, S. Tebaldini, M. Mariotti d'Alessandro and L. Villard, "Relating P-band synthetic aperture radar tomography to tropical forest biomass," *IEEE Transactions on Geoscience and Remote Sensing*, vol. 52, pp. 967–979, Feb. 2014. DOI: 10.1109/TGRS.2013.2246170 (cit. on p. 15).

[53] D. H. T. Minh, T. Le Toan, F. Rocca *et al.*, "SAR tomography for the retrieval of forest biomass and height: Cross-validation at two tropical forest sites in French Guiana," *Remote Sensing of Environment*, vol. 175, pp. 138–147, Mar. 2016. DOI: 10.1016/j.rse.2015.12.037 (cit. on p. 15).

[54] D. H. T. Minh, L. Villard, L. Ferro-Famil, S. Tebaldini and T. Le Toan, "P-band SAR tomography for the characterization of tropical forests," *2017 IEEE International Geoscience and Remote Sensing Symposium (IGARSS), Fort Worth, TX, USA*, pp. 5862–5865, Jul. 2017. DOI: 10.1109/IGARSS.2017.8128342 (cit. on p. 15).

[55] M. Mariotti d'Alessandro and S. Tebaldini, "Digital terrain model retrieval in tropical forests through P-band SAR tomography," *IEEE Transactions on Geoscience and Remote Sensing*, vol. 57, pp. 6774–6781, Sep. 2019. DOI: 10.1109/TGRS.2019.2908517 (cit. on p. 15).

[56] F. Banda, M. Mariotti d'Alessandro and S. Tebaldini, "Ground and volume decomposition as a proxy for AGB from P-band SAR data," *Remote Sensing*, vol. 12, Jan. 2020. DOI: 10.3390/rs12020240 (cit. on p. 15).

[57] Y. N. Ngo, Y. Huang, D. H. T. Minh, L. Ferro-Famil, I. Fayad and N. Baghdadi, "Tropical forest vertical structure characterization: From GEDI to P-band SAR tomography," *IEEE Geoscience and Remote Sensing Letters*, vol. 19, 2022. DOI: 10.1109/LGRS.2022.3208744 (cit. on p. 15).

[58] N. Ramachandran, S. Saatchi, S. Tebaldini, M. M. d'Alessandro and O. Dikshit, "Mapping tropical forest aboveground biomass using airborne SAR tomography," *Scientific Reports*, vol. 13, Dec. 2023. DOI: 10.1038/s41598-023-33311-y (cit. on p. 15).

[59] I. Hajnsek, M. Pardini, R. Horn *et al.*, "SAR imaging of tropical African forests with P-band multibaseline acquisitions: Results from the AfriSAR campaign," *2016 IEEE International Geoscience and Remote Sensing Symposium (IGARSS), Beijing, China*, pp. 7521–7523, Jul. 2016. DOI: 10.1109/IGARSS.2016.7730961 (cit. on p. 15).

[60] M. Pardini, J. S. Kim, K. Papathanassiou and I. Hajnsek, "3-D structure observation of African tropical forests with multi-baseline SAR: Results from the AfriSAR campaign," *2017 IEEE International Geoscience and Remote Sensing Symposium (IGARSS), Fort Worth, TX, USA*, pp. 4288–4291, Jul. 2017. DOI: 10.1109/IGARSS.2017.8127950 (cit. on p. 15).

[61] M. Pardini, M. Tello, V. Cazcarra-Bes, K. P. Papathanassiou and I. Hajnsek, "L- a nd P-band 3-D SAR reflectivity profiles versus lidar waveforms: The AfriSAR case," *IEEE Journal of Selected Topics in Applied Earth Observations and Remote Sensing*, vol. 11, pp. 3386–3401, Oct. 2018. DOI: 10.1109/JSTARS.2018.2847033 (cit. on p. 15).

[62] X. Yang, S. Tebaldini, M. Mariotti d'Alessandro and M. Liao, "Tropical forest height retrieval based on P-band multibaseline SAR data," *IEEE Geoscience and Remote Sensing Letters*, vol. 17, pp. 451–455, Mar. 2020. DOI: 10.1109/LGRS.2019.2923252 (cit. on p. 15).

[63] T. Fatoyinbo, J. Armston, M. Simard *et al.*, "The NASA AfriSAR campaign: Airborne SAR and lidar measurements of tropical forest structure and biomass in support of current and future space missions," *Remote Sensing of Environment*, vol. 264, Oct. 2021. DOI: 10.1016/j.rse.2021.112533 (cit. on p. 15).

[64] L. M. H. Ulander, A. Gustavsson, P. Dubois-Fernandez *et al.*, "BIOSAR 2010 - A SAR campaign in support to the BIOMASS mission," *2011 IEEE International Geoscience and Remote Sensing Symposium (IGARSS), Vancouver, Canada*, pp. 1528–1531, Jul. 2011. DOI: `10.1109/IGARSS.2011.6049359` (cit. on p. 15).

[65] S. Tebaldini and F. Rocca, "Multibaseline polarimetric SAR tomography of a boreal forest at P- and L-bands," *IEEE Transactions on Geoscience and Remote Sensing*, vol. 50, pp. 232–246, Jan. 2012. DOI: `10.1109/TGRS.2011.2159614` (cit. on p. 15).

[66] M. Neumann, S. S. Saatchi, L. M. H. Ulander and J. E. S. Fransson, "Assessing performance of L- and P-band polarimetric interferometric SAR data in estimating boreal forest above-ground biomass," *IEEE Transactions on Geoscience and Remote Sensing*, vol. 50, pp. 714–726, 2012. DOI: `10.1109/TGRS.2011.2176133` (cit. on p. 15).

[67] M. J. Soja, G. Sandberg and L. M. H. Ulander, "Regression-based retrieval of boreal forest biomass in sloping terrain using P-band SAR backscatter intensity data," *IEEE Transactions on Geoscience and Remote Sensing*, vol. 51, pp. 2646–2665, 2013. DOI: `10.1109/TGRS.2012.2219538` (cit. on p. 15).

[68] E. Blomberg, L. M. H. Ulander, S. Tebaldini and L. Ferro-Famil, "Evaluating P-band TomoSAR for biomass retrieval in boreal forest," *IEEE Transactions on Geoscience and Remote Sensing*, vol. 59, pp. 3793–3804, May 2021. DOI: `10.1109/TGRS.2020.3020775` (cit. on p. 15).

[69] O. Frey and E. Meier, "Analyzing tomographic SAR data of a forest with respect to frequency, polarization, and focusing technique," *IEEE Transactions on Geoscience and Remote Sensing*, vol. 49, pp. 3648–3659, Oct. 2011. DOI: `10.1109/TGRS.2011.2125972` (cit. on p. 15).

[70] A. T. Caicoya, F. Kugler, M. Pardini, I. Hajnsek and K. Papathanassiou, "Vertical forest structure characterization for the estimation of above ground biomass: First experimental results using SAR vertical reflectivity profiles," *2014 IEEE Geoscience and Remote Sensing Symposium (IGARSS), Quebec City, QC, Canada*, pp. 1045–1048, Jul. 2014. DOI: `10.1109/IGARSS.2014.6946607` (cit. on p. 15).

[71] A. T. Caicoya, M. Pardini, I. Hajnsek and K. Papathanassiou, "Forest above-ground biomass estimation from vertical reflectivity profiles at L-band," *IEEE Geoscience and Remote Sensing Letters*, vol. 12, pp. 2379–2383, Dec. 2015. DOI: `10.1109/LGRS.2015.2477858` (cit. on p. 15).

[72] V. Cazcarra-Bes, M. Tello-Alonso, R. Fischer, M. Heym and K. Papathanassiou, "Monitoring of forest structure dynamics by means of l-band SAR tomography," *Remote Sensing*, vol. 9, Dec. 2017. DOI: `10.3390/rs9121229` (cit. on p. 15).

[73] M. Tello, V. Cazcarra-Bes, M. Pardini and K. Papathanassiou, “Forest structure characterization from SAR tomography at L-band,” *IEEE Journal of Selected Topics in Applied Earth Observations and Remote Sensing*, vol. 11, pp. 3402–3414, Oct. 2018. DOI: 10.1109/JSTARS.2018.2859050 (cit. on p. 15).

[74] M. Pardini, J. Armston, W. Qi *et al.*, “Early lessons on combining lidar and multi-baseline SAR measurements for forest structure characterization,” *Surveys in Geophysics*, vol. 40, pp. 803–837, Jul. 2019. DOI: 10.1007/s10712-019-09553-9 (cit. on p. 15).

[75] M. Pardini, K. P. Papathanassiou and F. Lombardini, “Impact of dielectric changes on L-band 3-d SAR reflectivity profiles of forest volumes,” *IEEE Transactions on Geoscience and Remote Sensing*, vol. 56, pp. 7324–7337, Dec. 2018. DOI: 10.1109/TGRS.2018.2850357 (cit. on p. 15).

[76] S. Tebaldini, M. Mariotti d’Alessandro, L. M. H. Ulander *et al.*, “TomoSense: A unique 3D dataset over temperate forest combining multi-frequency mono- and bi-static tomographic SAR with terrestrial, UAV and airborne lidar, and in-situ forest census,” *Remote Sensing of Environment*, vol. 290, p. 113 532, May 2023. DOI: 10.1016/j.rse.2023.113532 (cit. on pp. 15, 20).

[77] H. T. M. Dinh, S. Tebaldini, F. Rocca *et al.*, “TropiScat: Multi-temporal multi-polarimetric tomographic imaging of tropical forest,” *2012 IEEE International Geoscience and Remote Sensing Symposium (IGARSS), Munich, Germany*, pp. 7051–7054, Jul. 2012. DOI: 10.1109/IGARSS.2012.6351947 (cit. on p. 16).

[78] D. H. T. Minh, S. Tebaldini, F. Rocca *et al.*, “Vertical structure of P-band temporal decorrelation at the Paracou forest: Results from Tropiscat,” *IEEE Geoscience and Remote Sensing Letters*, vol. 11, pp. 1438–1442, 2014. DOI: 10.1109/LGRS.2013.2295165 (cit. on p. 16).

[79] A. Hamadi, C. Albinet, P. Borderies *et al.*, “Temporal survey of polarimetric P-band scattering of tropical forests,” *IEEE Transactions on Geoscience and Remote Sensing*, vol. 52, pp. 4539–4547, Aug. 2014. DOI: 10.1109/TGRS.2013.2282357 (cit. on p. 16).

[80] S. E. I. Essebtey, L. Villard, P. Borderies *et al.*, “Temporal decorrelation of tropical dense forest at C-band: First insights from the TropiScat-2 experiment,” *IEEE Geoscience and Remote Sensing Letters*, vol. 17, pp. 928–932, Jun. 2020. DOI: 10.1109/LGRS.2019.2937382 (cit. on p. 16).

[81] S. E. I. Essebtey, L. Villard, P. Borderies, T. Koleck, B. Burban and T. Le Toan, “Comparative study of temporal decorrelation at P, L and C-bands: First insights from the Tropiscat-2 experiment,” *2020 Mediterranean and Middle-East Geoscience and Remote Sensing Symposium (M2GARSS), Tunis, Tunisia*, pp. 246–249, Mar. 2020. DOI: 10.1109/M2GARSS47143.2020.9105253 (cit. on p. 16).

[82] S. E. I. Essebtey, L. Villard, P. Borderies, T. Koleck, B. Burban and T. Le Toan, "Long-term trends of P-band temporal decorrelation over a tropical dense forest-experimental results for the BIOMASS mission," *IEEE Transactions on Geoscience and Remote Sensing*, vol. 60, pp. 1–15, 2022. DOI: 10.1109/TGRS.2021.3082395 (cit. on p. 16).

[83] C. Albinet, P. Borderies, T. Koleck *et al.*, "TropiSCAT: A ground based polarimetric scatterometer experiment in tropical forests," *IEEE Journal of Selected Topics in Applied Earth Observations and Remote Sensing*, vol. 5, pp. 1060–1066, 2012. DOI: 10.1109/JSTARS.2012.2201917 (cit. on p. 16).

[84] C. Albinet, T. Koleck, T. Le Toan *et al.*, "First results of AfriScat, a tower-based radar experiment in African forest," *2015 IEEE International Geoscience and Remote Sensing Symposium (IGARSS), Milan, Italy*, pp. 5356–5358, Jul. 2015. DOI: 10.1109/IGARSS.2015.7327045 (cit. on p. 16).

[85] A. R. Monteith and L. M. H. Ulander, "Temporal survey of P- and L-band polarimetric backscatter in boreal forests," *IEEE Journal of Selected Topics in Applied Earth Observations and Remote Sensing*, vol. 11, pp. 3564–3577, Oct. 2018. DOI: 10.1109/JSTARS.2018.2814825 (cit. on p. 16).

[86] A. R. Monteith and L. M. H. Ulander, "A tower-based radar study of temporal coherence of a boreal forest at P-, L-, and C-bands and linear cross polarization," *IEEE Transactions on Geoscience and Remote Sensing*, vol. 60, pp. 1–15, 2022. DOI: 10.1109/TGRS.2021.3074098 (cit. on p. 16).

[87] L. M. H. Ulander and A. R. Monteith, "Time series of P- and L-band forest backscatter from BorealScat," *2017 IEEE International Geoscience and Remote Sensing Symposium (IGARSS), Fort Worth, Texas, USA*, pp. 4310–4313, Jul. 2017. DOI: 10.1109/IGARSS.2017.8127955 (cit. on p. 16).

[88] L. M. H. Ulander, A. R. Monteith, M. J. Soja and L. E. B. Eriksson, "Multiport vector network analyzer radar for tomographic forest scattering measurements," *IEEE Geoscience and Remote Sensing Letters*, vol. 15, pp. 1897–1901, Dec. 2018. DOI: 10.1109/LGRS.2018.2865673 (cit. on p. 16).

[89] J. J. Ruiz, R. Vehmas, J. Lemmetyinen *et al.*, "SodSAR: A tower-based 1–10 GHz SAR system for snow, soil and vegetation studies," *Sensors*, vol. 20, p. 6702, Nov. 2020. DOI: 10.3390/s20226702 (cit. on p. 16).

[90] J. Lemmetyinen, J. J. Ruiz, J. Cohen *et al.*, "Attenuation of radar signal by a boreal forest canopy in winter," *IEEE Geoscience and Remote Sensing Letters*, vol. 19, pp. 1–5, 2022. DOI: 10.1109/LGRS.2022.3187295 (cit. on p. 16).

[91] J. J. Ruiz, J. Lemmetyinen, J. Lahtinen *et al.*, "Investigation of cryosphere processes in the boreal forest zone using ground-based SAR," *2022 52nd European Microwave Conference (EuMC), Milan, Italy*, pp. 83–86, Sep. 2022. DOI: 10.23919/EuMC54642.2022.9924473 (cit. on p. 16).

[92] L. M. H. Ulander, A. R. Monteith and J. E. S. Fransson, "Development and initial evaluation of the tower-based BorealScat-2 P-and L-band tomographic SAR," *2023 IEEE International Geoscience and Remote Sensing Symposium (IGARSS), Pasadena, CA, USA*, 2023 (cit. on p. 24).